Modeling vibroacoustic systems involving cascade open cavities and micro-perforated panels

Xiang Yu and Li Cheng[a)]
Department of Mechanical Engineering, The Hong Kong Polytechnic University, Hung Hom, Kowloon, Hong Kong

Jean-Louis Guyader
Laboratoire Vibrations-Acoustique, INSA Lyon, 25 bis, avenue Jean Capelle, 69621 Villeurbanne Cedex, France

(Received 22 April 2014; revised 10 June 2014; accepted 16 June 2014)

While the structural-acoustic coupling between flexible structures and closed acoustic cavities has been extensively studied in the literature, the modeling of structures coupled through open cavities, especially connected in cascade, is still a challenging task for most of the existing methods. The possible presence of micro-perforated panels (MPPs) in such systems adds additional difficulties in terms of both modeling and physical understanding. In this study, a sub-structuring methodology based on the Patch Transfer Function (PTF) approach with a Compound Interface treatment technique, referred to as CI-PTF method, is proposed, for dealing with complex systems involving cascade open/closed acoustic cavities and MPPs. The co-existence of apertures and solid/flexible/micro-perforated panels over a mixed separation interface is characterized using a compound panel subsystem, which enhances the systematic coupling feature of the PTF framework. Using several typical configurations, the versatility and efficiency of the proposed method is illustrated. Numerical studies highlight the physical understanding on the behavior of MPP inside a complex vibroacoustic environment, thus providing guidance for the practical design of such systems.
 [http://dx.doi.org/10.1121/1.4887442]

PACS number(s): 43.50.Gf, 43.55.Rg, 43.20.Tb [NX] Pages: 659–670

I. INTRODUCTION

Acoustic cavities, either partially or completely surrounded by vibrating structures, are commonly seen in various applications. Typical examples include vehicle and aircraft cabins, double-glazed windows, acoustic silencers, music instruments, etc. A closed cavity typically refers to an air volume enclosed by a continuous and closed boundary, while an open cavity has air aperture over part of the boundary surface, allowing direct interaction between the interior and exterior acoustic domains. The problem of a closed cavity with a surrounding flexible structure has been extensively studied in the literature.[1–5] For example, Dowell *et al.*[1] proposed a modal-based acoustoelasticity framework for dealing with such systems, and, in particular, investigated a rectangular cavity with a flexible wall. Fuller and Fahy[2] analyzed the sound wave propagation and energy distribution in an elastic cylindrical shell. Pan *et al.*[3] studied the sound transmission into an acoustic enclosure through a vibrating plate. Cheng *et al.*[4] examined a mechanically linked double-wall structure with a sandwiched acoustic cavity. Dijckmans *et al.*[5] simulated the transmission loss of multilayered lightweight structures using a transfer matrix method. The common point among these studies is that the acoustic cavities are closed without any aperture, thus the energy transmitted into the cavity interior is entirely through the flexural vibration of the structural boundary.

However, closed cavities only represent a limited number of practical applications. A more general system may comprise open acoustic cavities, where the separation interface between acoustic media can be both structural and acoustical. Since the coupling through the structure and the aperture needs to be treated separately, the direct application of the aforementioned techniques is not feasible. A representative example is illustrated in Fig. 1, in which multiple mixed separations, comprising rigid/flexible structure, air aperture, and micro-perforated panels (MPPs), are connected in cascade through open cavities. In principle, the acoustic domains on either end can be of any type, although rigid ducts are used in the figure for illustration purpose.

It has been demonstrated in the literature that sub-structuring approaches can best handle multilayered subsystems connected in series. In this paper, an improved Patch Transfer Function (PTF) approach[6–10] is proposed, with a number of added features specific to the handling of mixed separation between open cavities and the presence of micro-perforates. The so-called "patch" refers to the small surface area segmenting each coupling surface, on which the transfer functions describing the sound pressure and velocity relationships can, *a priori*, be determined. The coupling between the sub-divided domains is performed by manipulating these pre-calculated patch transfer functions (subsystem PTFs) under the superposition principle of linear system. In such a manner, multiple

a)Author to whom correspondence should be addressed. Electronic mail: li.cheng@polyu.edu.hk

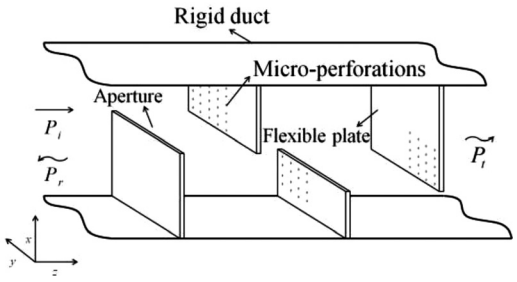

FIG. 1. Multiple mixed separations of flexible plate, aperture, and MPP connecting open acoustic cavities in cascade.

subsystems connected in series can be pieced together layer by layer.

However, the existing PTF framework is not efficient in handling open cavities. In order to tackle this difficulty, this paper presents a new "structuralized" formulation of the air aperture, with the latter being considered as an equivalent structural component (virtual panel).[11] Thus, by combining the structural part and the aperture into a single structural subsystem, referred to as "compound panel" hereafter, the coupling between the two acoustic domains can be characterized by an equivalent structural path, such converting a system with parallel connections into one with serial connections.

From a different perspective, the system complexity may also be due to the presence of other non-conventional structural/acoustic elements like MPPs. A typical MPP consists of a sheet metal with a lattice of sub-millimeter size perforation.[12] With appropriate perforation ratio, a MPP provides high acoustic resistance and low acoustic reactance, necessary for an effective sound absorption. Because of its appealing features such as cleanable, fiber-free and non-combustible, MPPs have found their use in a wide range of practical applications.[13–20] For example, Kang and Brocklesby[13] investigated the feasibility of applying MPP absorbers in ventilated window system. Allam and Åbom[14] proposed a new type of silencer based on MPP with slit holes. Wang *et al.*[15] developed a hybrid silencer using lightweight MPPs coupled with side-branch cavities. Bravo *et al.*[16,17] discussed the sound absorption and transmission of flexible MPPs and MPPs backed by a flexible plate. Liu and Herrin[18] studied the effect of MPP absorption in acoustic enclosure by partitioning the backing cavity. It has been demonstrated through these studies that the performances of MPPs can be strongly affected by their surrounding environment, which significantly differs from the impedance tube setting. This indicates that accurately predicting the behavior of MPPs inside complex environment requires fully coupled vibroacoustic modeling tools which consider the MPP as an integrated component of the system. In this study, the existence of micro-perforations over the structure is treated using an equivalent mobility method, which averages the effect of air-mass motion inside the holes and the flexural vibration of plate frame. The equivalent mobility of MPP is then combined with air aperture and other structural components to fully describe a compound panel subsystem.

In the following sections, the proposed sub-structuring framework is first formulated, together with the compound panel subsystem treatment and MPPs. Heavily relying on Compound Interface treatment under the PTF framework, the proposed method is therefore referred to as CI-PTF method. Using the proposed method, various representative examples are explored to demonstrate the capability and the flexibility of the proposed formulation. Among these examples, the coupling between open cavities in cascade, as well as the behavior of MPP absorbers inside complex working environment, is discussed and the underlying physics are revealed.

II. FORMULATION

The CI-PTF framework is first formulated. Consider a typical elementary cavity-separation-cavity system as shown in Fig. 2. Two open acoustic cavities are connected through a mixed separation comprising flexible panel, aperture, and MPP. This elementary system can serve as a basic building block to handle more complex configurations such as the one shown in Fig. 1, which can be constructed by connecting multiple such elementary systems in series. As illustrated in Fig. 2, the system is first decoupled into structural and acoustic subsystems, and each coupling surface is segmented into N small elementary surfaces called patches.[6,7] The subsystem patch transfer functions (PTFs) are defined as the pressure or velocity response at a receiving patch due to an excitation at another patch. More specifically, they are mainly classified into two categories: Patch mobility Y_{ij}^s for vibrating structures and patch impedance Z_{ij}^a for acoustic domains,

$$Y_{ij}^s = \frac{\bar{V}_i^s}{\bar{F}_j^s}, \quad \text{where} \quad \bar{V}_i^s = \frac{1}{S_i}\int_{s_i} V^s dS_i \quad \text{and} \quad \bar{F}_j^s = \frac{1}{S_j}\int_{s_j} F^s dS_j,$$
$$Z_{ij}^a = \frac{\bar{F}_i^a}{\bar{V}_j^a}, \quad \text{where} \quad \bar{V}_j^a = \frac{1}{S_j}\int_{s_j} V^a dS_j \quad \text{and} \quad \bar{F}_i^a = \int_{s_i} P^a dS_i, \tag{1}$$

where i and j denote the receiving and exciting patch, S_i and S_j are the corresponding patch surface area, superscripts s and a represent the corresponding structural and acoustic quantities, respectively. For the structural patch mobility, Y_{ij}^s is defined as the mean normal velocity on a receiving patch i resulted from a unit normal force imposed on patch j, and the acoustic impedance Z_{ij}^a is defined as the integration of

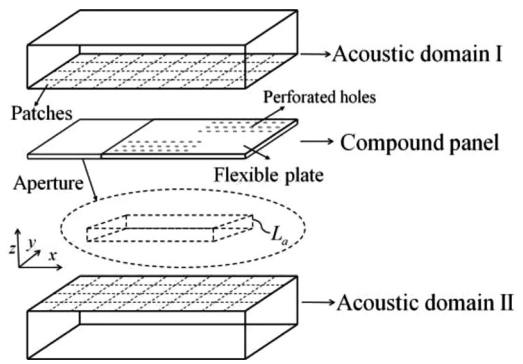

FIG. 2. Sub-structuring framework of the proposed PTF approach.

mean acoustic pressures on patch i due to an imposed unit velocity on exciting patch j. Note that PTFs of each subsystem can, *a priori*, be calculated before the assembly to form a set of database.

The mixed separation as shown in Fig. 2 consists of structural (flexible panel), acoustical (aperture), as well as mixed (MPP) components, which normally requires different treatment. This could jeopardize the systematic feature of sub-structuring techniques in dealing with complex systems. To tackle the problem, two techniques are proposed to empower the original PTF framework with the ability of handling such mixed separations, namely, the virtual panel treatment for the aperture, and the equivalent mobility treatment for the MPP. It is anticipated that if the mixed separations can be characterized using a single structural subsystem, the parallel connection between the open cavities can be converted into a serial one.

The virtual panel treatment to "structuralize" an air aperture is formulated as follows: consider an aperture of small thickness L_a connecting two open acoustic cavities in Fig. 2, the pressure field inside the aperture can be expressed in terms of two oppositely propagating acoustic waves,[21]

$$p_a(x,y,z) = \sum_n a_a^n \psi_a^n (e^{-jk_z^n z} + \hat{\varepsilon}^n e^{jk_z^n z}), \tag{2}$$

where a_a^n is the nth modal amplitude of the aperture; ψ_a^n is the corresponding cross-sectional eigenfunction; z axis defines the thickness direction; $\hat{\varepsilon}^n$ is the ratio between the coefficients of the forwarding and back-warding acoustic waves; k_z^n is the wave number along the z axis as $k_z^n = \sqrt{(\omega/c_0)^2 - (k_x^n)^2 - (k_y^n)^2}$, where k_x^n and k_y^n are the wave number according to the cross-sectional eigenfunction.

When the thickness of the air aperture is much smaller than the acoustic wavelength of interest, the through-thickness velocity fluctuations of the air particles should not be very drastic.[11] Thus, an averaged through-thickness velocity $\bar{V}_z$ can be assumed to characterize the pressure gradient in the z axis according to the momentum equation

$$\frac{\partial p_a}{\partial z} = -j\rho_0 \omega \bar{V}_z. \tag{3}$$

Using the pressure gradient at the front surface where $z = 0$, $\bar{V}_z$ is expressed as

$$\overline{V_z} = \sum_n \frac{a_a^n k_z^n (1 - \hat{\varepsilon}^n)\psi_a^n}{\rho_0 \omega}. \tag{4}$$

The sound pressures at the back surface, i.e., $z = L_a$, can be obtained using a Taylor's series expansion with neglected second-order higher terms:

$$p_a(x,y,L_a) \approx p_a(x,y,0) + L_a \frac{\partial p_a}{\partial z}. \tag{5}$$

Therefore, given a pressure difference Δp on both sides of the aperture, one has

$$\frac{\Delta p}{L_a} = -\frac{\partial p_a}{\partial z}. \tag{6}$$

By substituting the averaged through-thickness velocity expression in Eq. (4) into the above equation, and making use of the orthogonality property of the cross-sectional modes, the resulted aperture modal amplitude a_a^n due to the pressure excitation is obtained as

$$a_a^n = \frac{\int_{S_a} \Delta p \psi_a^n dS_a}{jk_z^n L_a N_a^n (1 - \hat{\varepsilon}^n)}, \tag{7}$$

where $N_a^n = \int_{S_a} \psi_a^n \psi_a^{n'} dS_a$, S_a is the aperture surface area.

According to the definition of patch mobility in Eq. (1), the equivalent mobility of the aperture Y_a eventually becomes

$$Y_a = \frac{\bar{V}_i^a}{\bar{F}_j^a} = \left(\frac{1}{j\rho_0 \omega L_a s_i s_j}\right) \sum_n \frac{1}{N_a^n} \int_{S_i} \psi_a^n dS_i \int_{S_j} \psi_a^n dS_j. \tag{8}$$

The calculation of patch mobility of the flexible panel is rather straightforward based on the modal expansion theory, which is discussed in Appendix A. Comparing the expressions of aperture mobility and panel mobility [i.e., Eqs. (8) and (A4), respectively], it can be seen that the aperture mobility in the present form is equivalent to a vibrating structure, with structural density ρ_0, thickness L_a, and a frequency-dependent stiffness (not explicitly shown here). The effective thickness range allowing for a satisfactory prediction of the aperture treatment is typically smaller than $\frac{1}{4}$ of the minimum acoustic wavelength of interest.[11] This so-called "virtual panel treatment" tactically converts an acoustical connection between open cavities into an equivalent structural one.

To follow the same logic, the presence of the MPP is also included into the compound panel subsystem described previously. To this end, the well-known Maa's formula,[12] based on short narrow tube theory, is used for calculating the characteristic impedance of the perforated holes as

$$Z_h = \frac{32\eta t}{d^2}\left[\left(1 + \frac{k^2}{32}\right)^{1/2} + \frac{\sqrt{2}}{32} k \frac{d}{t}\right] + j\rho_0 \omega t \left[1 + \left(1 + \frac{k^2}{32}\right)^{-1/2} + 0.85\frac{d}{t}\right], \tag{9}$$

where ρ_0 is the air density; η is the air viscosity; $k = d\sqrt{\rho_0 \omega / 4\eta}$; σ, t, and d are the perforation ratio, panel thickness, and perforated hole diameter, respectively.

It has been demonstrated in the literature that the actual behavior of MPP is determined by the relative motion between the air mass inside holes and the panel frame.[15–17] Therefore, an accurate description of the MPP inside complex vibroacoustic environment requires the inclusion of MPP vibration.

Consider a piece of thin flexible MPP with perforated holes. Given the short distance between perforated holes compared to the acoustic wavelength of interest, the averaged MPP velocity (or the mean air particle velocity in the vicinity of its surface) V_{mpp} can be approximated by averaging the plate vibrating velocity V_p and that of the air mass inside the holes V_h as

$$V_{mpp} = (1-\sigma)V_p + \sigma V_h. \tag{10}$$

The pressure difference Δp across the MPP surface is contributed by the viscous force due to relative motion between holes and frame, and the inertial force due to air mass motion only,[10,17]

$$\Delta p = \mathrm{Re}\{Z_h\}(V_h - V_p) + i\mathrm{Im}\{Z_h\}V_h, \tag{11}$$

where Re{} and Im{} denote the real part and imaginary part of the hole impedance.

For the plate vibration part, its velocity according to Eq. (1) can be expressed as

$$V_p = Y_p F_p = Y_p(\Delta p \times s), \tag{12}$$

where s is the surface area of the segmented patch.

By incorporating Eqs. (10)–(12), the equivalent MPP mobility Y_{mpp} can be obtained as

$$Y_{mpp} = \frac{\Delta p \times s}{V_{mpp}} = \left[(1-\sigma) + \frac{\sigma \mathrm{Re}(Z_h)}{Z_h}\right] Y_p + \frac{\sigma}{sZ_h}, \tag{13}$$

or, in a more compact form,

$$Y_{mpp} = \mathrm{T} \times Y_p + \mathrm{M}, \tag{14}$$

where $\mathrm{T} = (1-\sigma) + \sigma \mathrm{Re}\{Z_h\}/Z_h$ represents the contribution from the structural vibration to the averaged MPP velocity, Y_p is the patch mobility of the flexible plate frame, $\mathrm{M} = \sigma/(sZ_h)$ is the equivalent mobility of the perforation holes, contributed by the air mass vibration.

Now, different components over a mixed separation as shown in Fig. 2 have been formulated accordingly, which include flexible plate mobility Y_p (Appendix A), equivalent aperture mobility Y_a [Eq. (8)], and MPP mobility Y_{mpp} [Eq. (13)]. Owing to the segmentation of patches using the PTF approach, the global mobility matrix of a mixed separation can be conveniently constructed by combining those components at different positions, forming a kind of compound panel subsystem as follows:

$$\begin{bmatrix} Y_a & 0 & 0 \\ 0 & Y_p & Y_{p\text{-}mpp} \\ 0 & Y_{mpp\text{-}p} & Y_{mpp} \end{bmatrix} \begin{Bmatrix} F_a \\ F_p \\ F_{mpp} \end{Bmatrix} = \begin{Bmatrix} V_a \\ V_p \\ V_{mpp} \end{Bmatrix}, \tag{15}$$

where $Y_{p\text{-}mpp}$ and $Y_{mpp\text{-}p}$ are the cross-coupling terms between the solid and micro-perforated part of the flexible panel. The null terms indicate that the coupling between the air aperture and structure is weak, due to the significant difference in their impedance.

As to the patch impedance Z_a for different acoustic domains, three typical cases are considered in this study, including acoustic cavity Z_c, semi-infinite field Z_r, and rectangular duct radiation Z_d. Their detailed formulations are summarized in Appendixes B–D, respectively.

After all these treatments, the PTF assembling procedure for the entire system shown in Fig. 2 can be performed by making use of the superposition principle of linear vibroacoustic systems. On one hand, patch velocities for the structural interface (compound panel) can be expressed as a sum of the initial velocity $\tilde{V}_s$ before the coupling, and the velocity resulted from the forces exerted by the coupled domains, calculated via structural PTFs. On the other hand, patch forces for the acoustic domains are the sum of initial force $\tilde{F}$ before the coupling, and the force induced by the structural vibration, calculated via acoustic PTFs,

$$\begin{aligned} V_s &= \tilde{V}_s + Y_s(F_1 + F_2) && \text{compound panel,} \\ F_1 &= \tilde{F}_1 + Z_1 V_1 && \text{acoustic domain I,} \\ F_2 &= \tilde{F}_2 + Z_2 V_2 && \text{acoustic domain II.} \end{aligned} \tag{16}$$

The above equations are fully coupled in nature. By adding continuity conditions of normal patch velocities at the connecting patches $V_1 = V_2 = V_s$, the response of the compound panel can be calculated as

$$V_s = \frac{\tilde{V}_s + Y_s(\tilde{F}_1 + \tilde{F}_2)}{I - Y_s(Z_1 + Z_2)}, \tag{17}$$

where subscripts 1 and 2 represent acoustic domains I and II, respectively.

For multiple mixed separations connected via open cavities in cascade, such as the one shown in Fig. 1, or systems involving complex loadings or attachments, the above modeling principle is still applicable. It is worth mentioning again that the pre-calculated subsystem PTFs, stored as databases, can be flexibly manipulated for constructing any desired system configuration, which could significantly save the modeling effort compared with traditional global modeling approaches.

Once the velocity response of each coupled interface is obtained, other parameters, such as the sound transmission loss (TL), can be evaluated by $\mathrm{TL} = 10\log_{10}(1/\tau)$, where τ is the ratio between the radiated and incident sound power $\tau = \Pi_{rad}/\Pi_{inc}$. The incident sound power Π_{inc} corresponding to a normal plane wave excitation with pressure amplitude p_0 is

$$\Pi_{inc} = \frac{|p_0|^2}{2\rho_0 c_0} S_{inc}, \tag{18}$$

where S_{inc} is the area of the incident surface. Also, for the radiated sound power Π_{rad},

$$\Pi_{\mathrm{rad}} = \frac{1}{2}\int_{s_{\mathrm{rad}}} \mathrm{Re}\{P_{\mathrm{rad}} \times V^*_{\mathrm{rad}}\} dS_{\mathrm{rad}}, \tag{19}$$

where P_{rad} is the radiated sound pressure at each patch, calculated via radiation impedance Z_r; S_{rad} is the area of the radiation surface; the asterisk for the patch velocity denotes the complex conjugate.

III. APPLICATION EXAMPLES

The proposed CI-PTF method can be applied to a wide spectrum of structural-acoustic problems, some of which are investigated in the following sections as illustrative examples.

A. Baffled double-glazed panel system

The first application example considers a double-glazed panel system embedded in an infinite baffle, where two vibrating plates separated by an acoustic cavity are exposed to semi-infinite acoustic fields on both sides. This example could validate the proposed PTF framework, as well as the subsystem treatment including the flexible panel, acoustic cavity, and semi-infinite acoustic domains. As shown in Fig. 3, the upper panel is excited by a plane wave of normal incidence with a unit pressure amplitude $p_0 = 1$, resulting in an incident sound pressure field above the panel as $p_i = 2p_0 + p_i^{\text{rad}}$, with $2p_0$ being the blocked acoustic pressure and p_i^{rad} the radiated sound pressure due to the panel vibration. Similarly, the radiated acoustic field below the lower panel is written as $p_r = p_r^{\text{rad}}$. In the simulation, the two plates are assumed to be identical, made of aluminum with a cross-section of $0.5\,\text{m} \times 0.3\,\text{m}$, and a thickness of 1 mm. Both plates are assumed to be simply supported along the four edges for the sake of simplicity. The sound pressure field inside the rectangular cavity with a depth of 0.6 m is expressed in terms of the rigid-walled acoustic modes, with detailed formulation given in Appendix B.

The cavity between the two panels is treated in several ways. The simplest one (case 1) is to consider the cavity between the two panels as a subsystem as a whole. This case serves as the benchmark case to verify the subsystem PTFs, including flexible panel mobility Y_p [Eq. (A4)], cavity impedance Z_c [Eq. (B5)], and radiation impedance Z_r [Eq. (C1)]. In Fig. 4, the predicted TL using the proposed approach is presented, which exhibits strong resonant pattern. The first dip at 35 Hz corresponds to the first panel mode, while the second dip at 62 Hz being the panel-cavity coupled resonance, and the next dip at 114 Hz a panel-controlled resonance. The same system was investigated previously using finite-element method (FEM).[22] Although not shown here, a perfect agreement is found to exist between the present result and that reported using FEM.[22]

To further verify the accuracy of the aperture treatment using the present example, two more cases with sub-divided cavities (0.3 m in thickness each) are tested with results shown in Fig. 4: case 2 directly connects the sub-cavities by using continuity of pressures and velocities over the separating surface, while case 3 inserts a virtual panel (of 1 mm thick) in the middle, resulting in a system involving three structural subsystems (two real panels and one virtual panel) coupled through two cavities. As shown in Fig. 4, the good agreement between case 1 and case 2 indicates that adopting

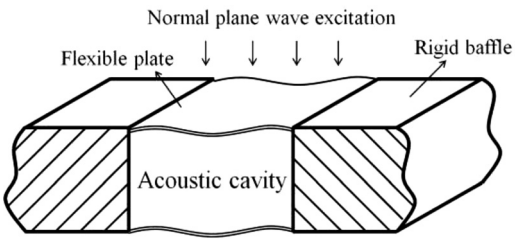

FIG. 3. Double-glazed panel system in an infinite baffle under plane wave incidence.

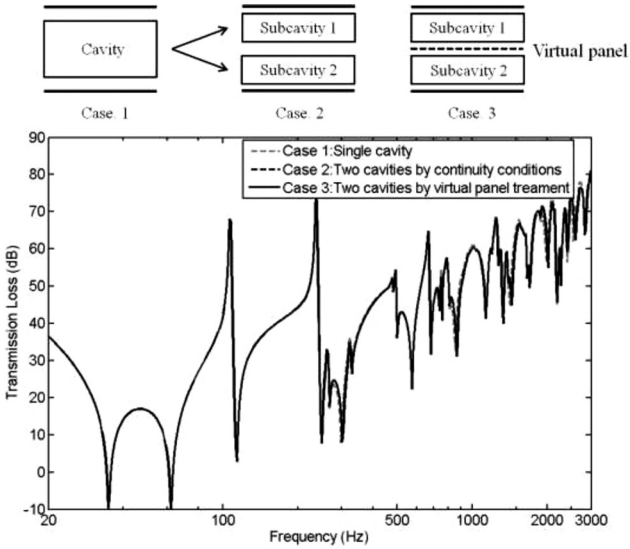

FIG. 4. Transmission loss of the system shown in Fig. 3 calculated using the proposed approach.

rigid-walled acoustic modes in the calculation is accurate even though the cavity is sub-divided into "open" cavities. This also confirms the cavity impedance treatment as formulated in Appendix B. For case 3, it can be seen that using virtual panel for aperture modeling results in very good agreement with previous two cases, which verifies the validity of the proposed virtual panel treatment.

B. Expansion chamber muffler

Expansion chamber mufflers[23–25] as noise control devices are widely used. Using the proposed sub-structuring approach, the TL of such mufflers is studied. Figure 5 shows a 2-D empty expansion chamber with infinite-long inlet and outlet ducts, where the corresponding dimensions are as sketched. The well-known 1-D theory based on plane wave assumption gives[24]

$$\text{TL} = 10\log_{10}\left(1 + 0.25\left(m - \frac{1}{m}\right)^2 \sin^2(kl)\right), \qquad (20)$$

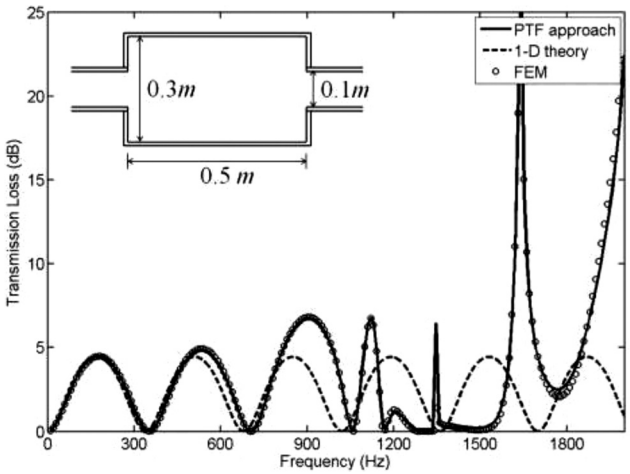

FIG. 5. Transmission loss of an empty expansion chamber, with comparison to 1-D theory and FEM analysis.

where m is the expansion ratio, l is the chamber length, and k is the wave number. The calculated TL using this analytical formula shows periodic dome-like behavior throughout the frequency range, with TL maxima appearing at $f = (2n-1)c_0/4l$ and minima at $f = nc_0/2l$, $n = 1, 2, 3, \ldots$.

The proposed PTF approach is employed, where the entire system is sub-divided into inlet duct, chamber cavity, and outlet duct. In principle, the coupling between these subsystems can be treated using either continuity descriptions of pressures and velocities, or the structuralized aperture treatment based on the compound panel. The latter is adopted here due to the flexibility it offers. In Fig. 5, the predicted TL using the proposed PTF approach shows excellent agreement with the finite element result using commercial software COMSOL Mutiphysics, while the PTF approach is shown to be more computational efficient.[11] The influence of the multi-dimensional waves at frequencies higher than the cut-off frequency of the muffler ($f_c = 570\,\text{Hz}$) is also obvious, which leads to the complete break-down of the plane wave model.

To demonstrate the capability of the proposed formulation, Fig. 6 further considers another two configurations of multi-chamber muffler with extra internal partitions inside the empty chamber. The original chamber length $l = 0.5\,\text{m}$ is sub-divided by one or four pairs of partial partitions, forming a serial connection of multiple open cavities. The added partitions are all rigid. Using the PTF approach described in Sec. II, the system involving partial partitions (treated as compound panels comprising a solid part and an air aperture part) connecting sub-cavities in cascade in the longitudinal direction is modeled, where the corresponding subsystem PTFs are stored in a pre-calculated database. In this way, structural complexities such as extra partitions or even more complex arrangements do not pose any technical difficulty in using the proposed method. As shown in Fig. 6, TL comparisons between the PTF approach and FEM analyses again demonstrate the calculation accuracy of the model. Compared with an empty chamber used in Fig. 5, the added partitions significantly alter the periodic TL pattern of an empty expansion chamber, even resulting in very high TL at certain frequency band. Both the height and position of the enhanced TL regions seem to be dependent on the number of partitions. This observation suggests that room exists for tuning and optimizing the performance of such mufflers through the use of internal partitions, although it is beyond the scope of the present study. The design cost using the proposed substructuring method is very low due to the modular nature of the method.

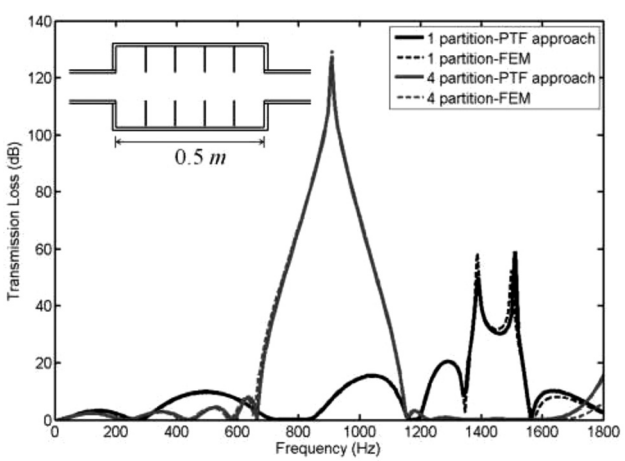

FIG. 6. Transmission loss of expansion chambers with additional internal partitions.

C. Sound radiation from a partially opened cavity

The proposed compound panel treatment not only provides an efficient tool for dealing with coupled open cavities, but also offers the opportunity for investigations into some typical vibroacoustic problems, where both structural and acoustical couplings between acoustic media co-exist. Figure 7 shows a typical example involving a partially opened acoustic cavity with a point source inside. The separation between the interior and exterior acoustic fields can be any combination of rigid/flexible plate and aperture. This system may represent a room with an opening, loudspeaker system, partial noise insulation enclosure, etc.[26] Using the PTF approach, the exterior domain is described as a semi-infinite radiation field using Rayleigh's integral (Appendix C); a single compound panel subsystem is used to describe the mixed separations connecting the interior and exterior fields.

To validate the model, the sound pressure level (SPL) at a receiving point as shown in Fig. 7 is calculated, and it is compared to that obtained from FEM. In the simulation, the acoustic cavity has a dimension of $1\,\text{m}(x) \times 0.2\,\text{m}(y) \times 0.8\,\text{m}(z)$, and a plate [of width $0.8\,\text{m}(x)$] covers $\frac{4}{5}$ of the open cavity. The plate is first assumed to be rigid. A sound source is located at $(0.05, 0.01, 0.1)$, and the receiving point at $(0.9, 0, 1.1)$. Note that the radiation field in FEM model is artificially approximated by constructing an outer enclosure with sound absorbing boundary conditions, whose impedance equals to the air impedance $\rho_0 c_0$. Using Rayleigh's integral, the radiated sound pressure P_p^r at the receiving point p due to a vibrating patch j (over the aperture area) of the compound panel can be calculated using the radiation impedance Z_{rpj}, which is defined as

$$Z_{rpj} = \frac{P_p^r}{\bar{V}_j^r} = \frac{1}{2\pi} j\rho_0\omega \frac{e^{-jkd_{pj}}}{d_{pj}} s_j, \tag{21}$$

where d_{pj} is the distance between the receiving point and center of the radiating patch area S_j. Figure 8 compares the

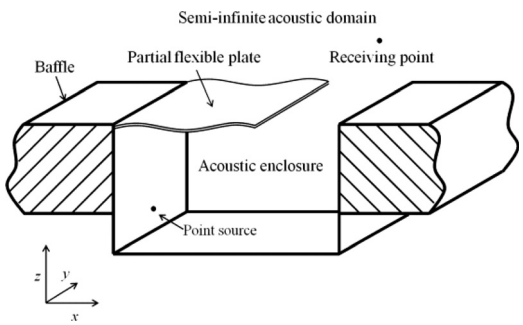

FIG. 7. Sound radiation from a partially opened acoustic cavity.

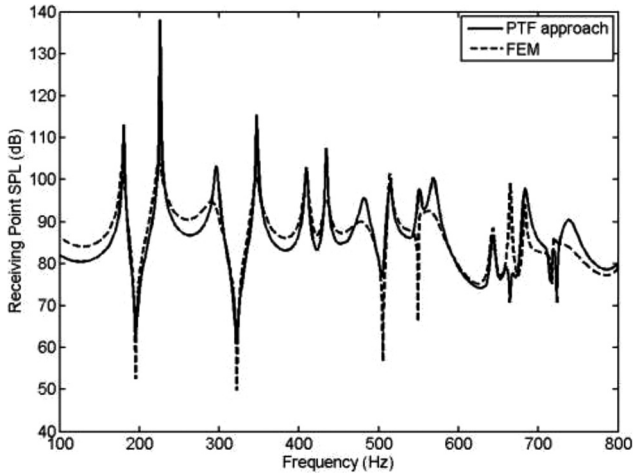

FIG. 8. SPLs at the receiving point calculated using PTF approach and FEM.

SPLs at the receiving point calculated via PTF approach and FEM. It can be seen that the two curves generally agree well over the frequency range, despite some noticeable discrepancies, which are mainly attributed to the boundary approximation made in the FEM model.

In Fig. 9, the visualized sound pressure fields using the PTF approach are presented at an arbitrary frequency of 600 Hz, where (a) and (b) correspond to the complete and half opening cases, respectively. It can be seen that the sound pressures in both cases are continuous across the aperture, as expected. The exterior radiation field is typically in a scattering pattern, and the interior cavity domain shows strong modal behavior.

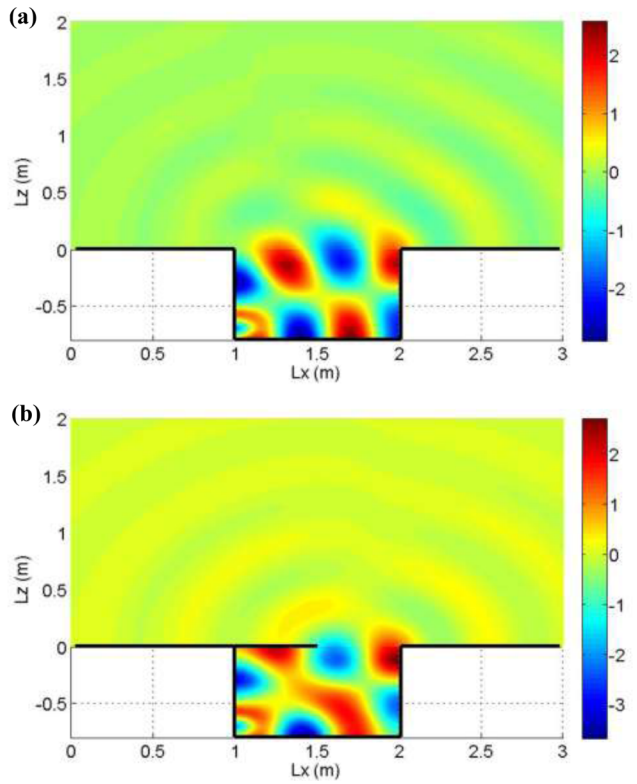

FIG. 9. (Color online) Sound pressure field visualizations: (a) a complete opening; (b) a half opening.

As to the effect of structural vibration over the mixed separation, Fig. 10 compares two cases with rigid and flexible plates, respectively, both covering $\frac{4}{5}$ of the cavity opening. In the rigid case, the interaction between acoustic media can only take place through the aperture, as evidenced by a continuous pressure variation over the aperture while an obvious pressure discontinuity across the rigid plate. For the flexible case at its structural resonance $f = 128$ Hz, however, the high pressure jump blocked by the partial structure is weakened, due to a significant increase in the structural mobility. Therefore, the interaction between acoustic media takes place through a combination of both structural and acoustical connections. Note that the curved panel sketched in Fig. 10(b) is intended to indicate that the panel is flexible. It does not correspond to its actual deflection shape. Using near-field acoustic holography in the experimental work,[26] similar observations were obtained, in agreement with the present findings.

D. MPP inside complex vibroacoustic environment

The three-dimensional system shown in Fig. 1 is considered here, in which staggered partial partitions or MPPs are connected in cascade through open acoustic cavities. The system can actually represent a wide range of practical applications, such as MPP backed by air layer and flexible plate,[16] double-glazed ventilation window[27] and with MPP absorbers,[13] mufflers with internal partitions[24] or MPPs as sound absorbing panels,[14] etc. Using the proposed formulation, different combinations of flexible plates, apertures and MPPs are characterized into a compound panel subsystem,

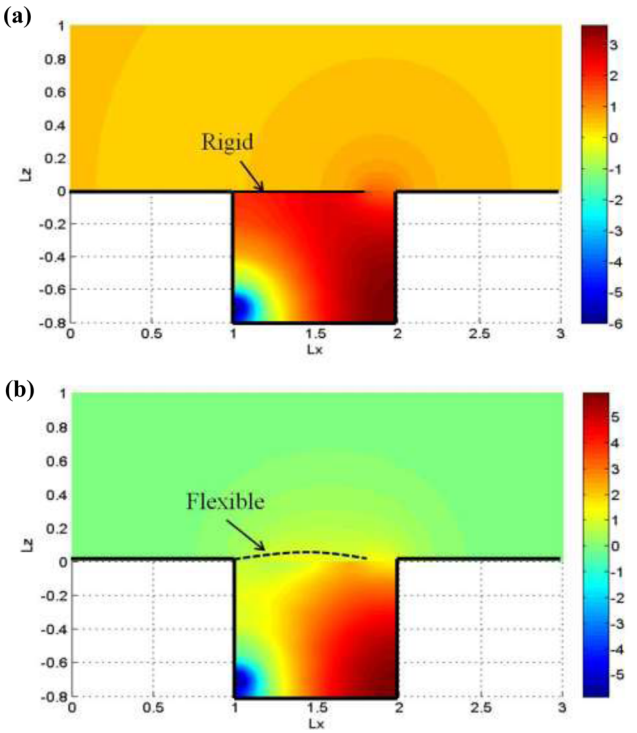

FIG. 10. (Color online) Effect of structural resonance on the sound radiation: (a) the partial structure is rigid; (b) the partial structure is flexible at its resonance $f = 72$ Hz (the deflection shape is only to show the panel is flexible).

allowing a flexible description of the separation layers. In the inlet duct, the system is excited by a normal incident plane wave. The reflected sound waves, as well as the transmitted waves in the outlet duct, are calculated using duct radiation impedance Z_d (Appendix D).

As a starting point, Fig. 11 compares TL curves for three cases: Case 1 as benchmark has double staggered panels; case 2 adds two partial MPPs in parallel alignment with outer panels; case 3 in staggered alignment, respectively. In the simulation, the cross-section of the rigid duct is $0.5\,\mathrm{m}(x) \times 0.5\,\mathrm{m}(y)$, and that of the partial panels (including MPPs) is $0.4\,\mathrm{m}(x) \times 0.5\,\mathrm{m}(y)$. The compound surface area is meshed into 10×10 patches to ensure the calculation convergence up to 3400 Hz,[6,7] and each panel in aluminum has a thickness of 2 mm, simply supported along the edges for the sake of simplicity. The open cavity is 1 m wide, evenly divided by two identical MPPs, having a hole diameter of 0.2 mm and perforation ratio of 1%.

Figure 11 shows that both cases with additional MPPs generally improve the TL performance as compared to case 1, where case 3 with staggered alignment seems to perform better than case 2 with parallel alignment at most frequencies. The corresponding sound pressure fields at $f = 480$ Hz are visualized in Fig. 12, where the sound pressure across the apertures are shown to be continuous. Inside the outlet duct, the radiated sound pressure level for the staggered case 3 is visibly lower, in agreement with the TL comparison in Fig. 11.

To demonstrate the effect of the MPP, the predicted TLs with/without micro-perforations in the staggered alignment case are compared in Fig. 13. Case A has two inner solid panels, which are replaced by two MPPs in case B. The TL curve of case A has been validated against a FEM model with good agreement (not shown here). For frequency range up to 3000 Hz with 300 calculation points, the computational time using the PTF approach is typically several minutes, while FEM analysis with 1×10^6 nodes generally takes one hour. When the system dimension is amplified by 5–6 times,

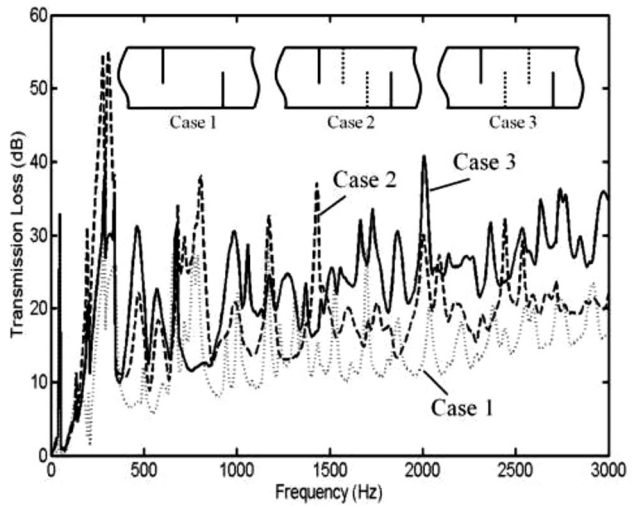

FIG. 11. TLs according to three cases: Case 1, double staggered panels; case 2, two additional MPPs in parallel alignment with outer panels; case 3, two MPPs in staggered alignment.

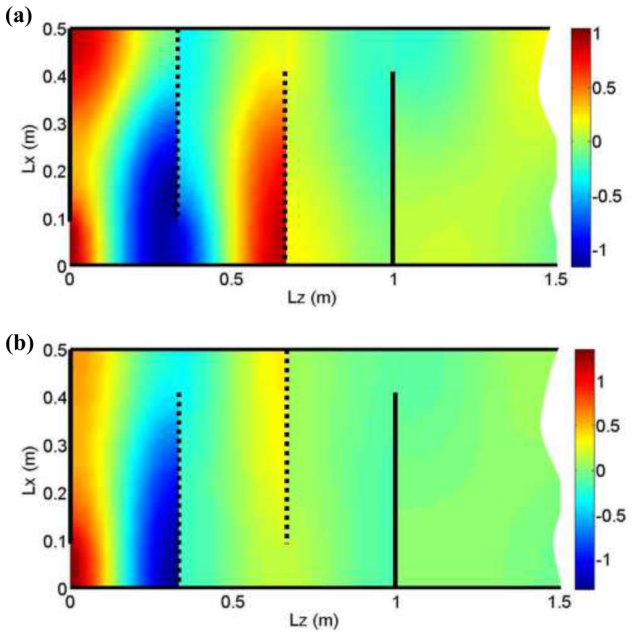

FIG. 12. (Color online) Visualization of sound pressure field: (a) parallel alignment case 2; (b) staggered alignment case 3.

analysis shows that PTF calculation has much better convergence at high frequencies than FEM.

Figure 13 shows that introducing micro-perforations allows lifting up the TL dips and reducing some TL peaks in case A, resulting in a more flattened and uniformly distributed TL curve. The lifted TL dips are mainly attributed to the MPP dissipation, which is equivalent to increasing the system damping. The original TL peaks in case A are due to the reactive effect of staggered partitions by creating internal area discontinuities, where the sound reflection is strong. With perforation holes, the sound pressures across the MPP surface become more continuous,[11] thus the TL peaks are seen to be reduced due to weakened reactive effect. Roughly, the introduction of MPPs leads to a 5 dB increase of the lower envelop of the TL curves, which is an appreciable improvement for broadband noise control applications.

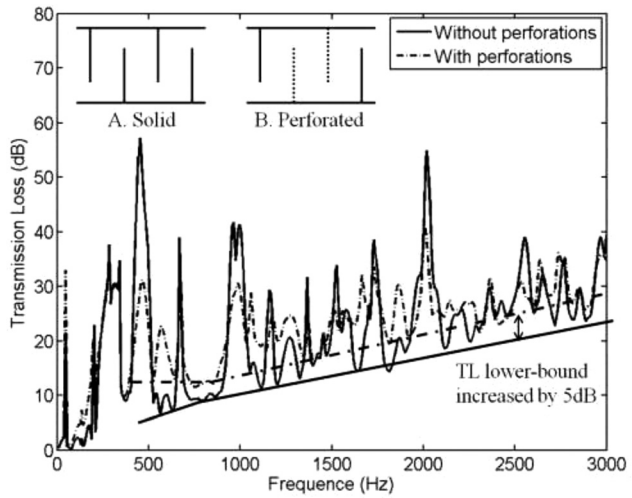

FIG. 13. Effect of MPP: Transmission loss with added inner panels with/-without perforations.

To quantify the energy dissipation by the first MPP at $L_z = 0.33$ m, an "absorption ratio" is defined as

$$\text{absorption ratio} = 1 - \frac{W_{\text{out}}}{W_{\text{in}}}, \tag{22}$$

where $W_{\text{in}} = \frac{1}{2}\int_{S_{\text{in}}} \text{Re}\{P_{\text{in}} \times V_{\text{in}}^*\} dS_{\text{in}}$ is the sound power entering the front surface of the box (Fig. 14), and $W_{\text{out}} = \frac{1}{2}\int_{S_{\text{out}}} \text{Re}\{P_{\text{out}} \times V_{\text{out}}^*\} dS_{\text{out}}$ is the transmitted sound power leaving the back surface. Note that the two surfaces are selected very close to each in the vicinity of the structural surface, in order to avoid null boundary velocities due to the use of the rigid-walled acoustic modes. It is anticipated that if no absorbing element is presented inside the prescribed box, this absorption ratio should be constantly zero.

Figure 14 shows the absorption ratio curves of the solid panel (Case A) and the MPP (Case B). For the solid panel case, the absorption ratio is constantly zero, indicating that the sound powers entering and leaving the enclosed box are equal as expected. With the MPP, the absorption ratio shows strong dependence on the frequency. In fact, the MPP is fully coupled to the surrounding vibroacoustic environment; its sound absorption exhibits extremely complex frequency-dependent behavior. One can surmise that a MPP cannot be treated as a local reactive component (like conventional sound absorption materials) in designing such systems. As a result, MPPs should be taken as an integrate part of the system and, for that, accurate, fully coupled modeling tools as the one presented in this study is definitely needed.

The influence of structural resonance on the sound transmission is shown by the plot of acoustic intensity vectors, which represents the time-averaged energy flux. Using the staggered case with four identical flexible panels as an example, Fig. 15(a) presents the intensity vectors at a low frequency of $f = 10$ Hz, where the energy flow mainly goes through the apertures and is blocked by the structures. Indeed, the apertures having lower acoustic impedance compared to the relatively strong structures allow the acoustic waves to penetrate through more easily. In Fig. 15(b), the

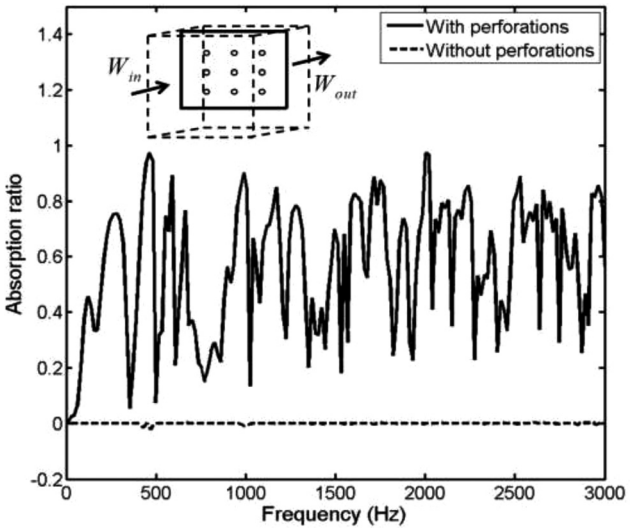

FIG. 14. Actual sound absorption ratio of a MPP inside the complex vibroacoustic environment.

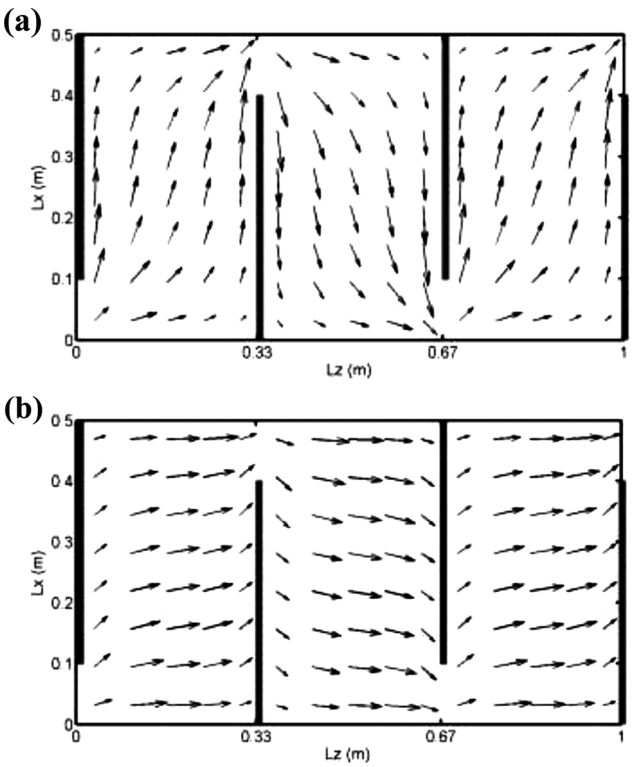

FIG. 15. Visualization of energy flow using sound intensity vectors: (a) $f = 10$ Hz, acoustic path dominant; (b) $f = 72$ Hz (panel resonance), both structural and acoustic paths.

intensity vectors at $f = 49$ Hz are plotted, corresponding to the first structural resonance of all panels. It can be seen that energy transmission through the cascade separation layers penetrates through the flexible panels to a larger extent, due to the significantly weakened structural impedance at the resonance. This phenomenon should be particularly noted when designing reactive silencers with internal partitions.[28] When the internal partitions are made of thin metal sheets, the overall noise attenuation ability of the silencers can be overestimated in simulation without considering the vibration effects but can be seriously compromised in practice.

So far, the capability of the proposed CI-PTF method has been demonstrated through several representative configurations. It should be noted, however, that although the current formulation, owing to its modular and patch average nature, can cover a much wider frequency range (low to mid-high) than other conventional methods such as FEM/BEM, the very high frequency end is still a problem. At high frequencies, energy based method such as Static Energy Analysis (SEA) is definitely more appropriate. Another limitation of the compound panel treatment is related to the geometry of the mixed interface. At its current version, the treatment is applicable to flat separation interfaces due to the mathematical treatment along the thickness direction.

IV. CONCLUSIONS

An improved PTF framework based on the substructuring principle is proposed to deal with complex vibroacoustic systems involving open acoustic cavities and microperforated elements connected in cascade. For a mixed

separation between cavities, the presence of air aperture is treated as a virtual vibrating panel, while the MPP is modeled using an equivalent mobility method. By doing so, different combination of rigid/flexible structure, aperture and MPP can be regrouped into a single compound panel subsystem. This treatment tactically converts the parallel connections between acoustic media into serial connections, thus overcoming some of the inherent difficulties of the PTF techniques in dealing with complex systems allowing both structural and acoustic sound transmissions. The updated PTF approach with upgraded Compound Interface (CI) features is referred to as CI-PTF method.

CI-PTF method simplifies the modeling procedure in handling mixed separations, thus allowing the exploration of a wide spectrum of challenging application examples. The accuracy and efficiency of the proposed framework, along with the subsystem treatments, are thoroughly validated through typical examples. The effects of structural vibration, partial opening, micro-perforation in typical vibroacoustic systems are investigated, allowing some fundamental physical understandings.

The efficiency and flexibility offered by CI-PTF method warrant its use in performing system optimization, for the better system design in practical applications. Regarding MPPs, their actual sound absorption performance is shown to be strongly dependent on the surrounding environment in which they are put in. This unequivocally advocates that a MPP cannot simply be considered as a locally reactive element in a complex working environment. Instead, it should be considered as an integrative part of the whole system, for which fully coupled modeling tools as the one presented in this study are definitely needed.

It is relevant to note that, in a broader sense, the proposed CI-PTF method is capable of tackling even more complex system configurations, such as irregular shaped or inhomogeneous subsystems, etc. Note that the calculation of subsystem PTFs is not confined to simple geometries using analytical expressions, while other methods such as FEM or even experimental measurements are also applicable to subsystems for real industrial applications.

ACKNOWLEDGMENT

The authors wish to acknowledge two grants from Research Grants Council of Hong Kong Special Administrative Region, China (Grant Nos. PolyU 5103/13E and PolyU152026/14E).

APPENDIX A: FLEXIBLE PANEL MOBILITY Y_S

The panel flexural vibration is governed by the Love-Kirchhoff equation as

$$D^*\nabla^4 w_p(x,y,t)+\rho_p h\frac{\partial w_p(x,y,t)}{\partial t^2}=\Delta p, \tag{A1}$$

where $w_p(x,y,t)$ is the panel transverse displacement, ρ_p, h, and D^* are the density, thickness, complex flexible rigidity of the panel, respectively.

Based on the modal expansion theory, $w_p(x,y,t)$ can be expanded in terms of modal coordinates as

$$w_p(x,y,t)=\sum_m a_p^m\Phi_p^m, \tag{A2}$$

where a_p^m is the mth modal amplitude of the panel, Φ_p^m is the corresponding modal shape function.

For classical boundary conditions such as simply supported, the eigenfunctions are analytically known.[7] While for other boundaries, a semi-analytical approach[29,30] can be used to obtain the corresponding eigenfunctions.

In a harmonic regime with an angular frequency ω, using the orthogonality property, the modal amplitude is obtained by multiplying the governing equation with an extra Φ_p^m and integrating over the surface,

$$a_p^m M_p^m(\omega_m^2-\omega^2)=\int_{S_p}\Delta p\Phi_p^m dS_p. \tag{A3}$$

Therefore, according to the definition in Eq. (1), the flexible panel mobility Y_p can be calculated as

$$Y_p=\frac{\bar{V}_i^p}{\bar{F}_j^p}=\sum_m\frac{j\omega}{M_p^m s_i s_j(\omega_m^2-\omega^2)}\int_{s_i}\Phi_p^m dS_i\int_{s_j}\Phi_p^m dS_j. \tag{A4}$$

APPENDIX B: ACOUSTIC CAVITY IMPEDANCE Z_C

The sound pressure field p_c inside an acoustic cavity coupled with a vibrating structure can be expanded into a series of eigenfunctions as

$$p_c(x,y,z)=\sum_r a_c^r\varphi_c^r, \tag{B1}$$

where a_c^r is the rth modal amplitude of the cavity, φ_c^r is the corresponding eigenfunctions.

For rectangular shaped cavity, rigid-walled acoustic modes as eigenfunctions are assumed for the sake of simplicity as

$$\varphi_c^r=\cos\left(\frac{r_x\pi}{L_x^c}x\right)\cos\left(\frac{r_y\pi}{L_y^c}y\right)\cos\left(\frac{r_z\pi}{L_z^c}z\right),\quad r_x,r_y,r_z=0,1,2,\ldots, \tag{B2}$$

where L_x^c, L_y^c, L_z^c are the cavity dimensions in the x, y, z directions, respectively.

The Green's formula together with Helmholtz equation is used to relate the variables and boundary condition terms in an integral equation,

$$\int_{V_c}(p_c\nabla^2\varphi_c^r-\varphi_c^r\nabla^2 p_c)dV_c=\int_{s_c}\left(p_c\frac{\partial\varphi_c^r}{\partial n}-\varphi_c^r\frac{\partial p_c}{\partial n}\right)dS_c. \tag{B3}$$

Substituting the pressure gradient of a vibrating boundary $\partial p_c/\partial n=-j\rho_0\omega\bar{V}_n$ into the above equation, the cavity modal amplitude can be calculated as

$$a_c^r N_c^r(k^2-k_r^2)=\int_{s_c}(j\rho_0\omega\bar{V}_n)\varphi_c^r dS_c. \tag{B4}$$

Then, according to Eq. (1), the patch impedance of the acoustic cavity is expressed as

$$Z_c = \frac{\bar{F}_i^c}{\bar{V}_j^c} = \sum_r \frac{j\rho_0\omega}{N_c^r(k^2 - k_r^2)} \int_{s_i} \varphi_c^r dS_i \int_{s_j} \varphi_c^r dS_j. \tag{B5}$$

APPENDIX C: SEMI-INFINITE RADIATION IMPEDANCE Z_r

For a vibroacoustic system embedded in an infinite baffle, the radiated sound pressure into the semi-infinite acoustic field can be calculated using radiation impedance. Using the PTF approach, a radiating patch impedance Z_r based on the Rayleigh's integral method is used. The segmentation of patches over the radiating surface is required to be smaller than the half acoustic wavelength of interest, thus each vibrating patch can be considered as a simple monopole source.[7,10]

The radiated sound pressure P^r is contributed by two parts, namely, the self-patch and cross-patch radiations. The corresponding components are defined as

$$\begin{aligned} Z_{rii}^P &= \frac{\bar{P}_i^r}{\bar{V}_i^r} = \rho_0 c_0 (1 - e^{-jka}), \\ Z_{rij}^P &= \frac{\bar{P}_i^r}{\bar{V}_j^r} = \frac{1}{2\pi} j\rho_0\omega \frac{e^{-jkd_{ij}}}{d_{ij}} s_j, \end{aligned} \tag{C1}$$

where a is the equivalent radius of a simple monopole source, by approximating the rectangular patches as circular ones. d_{ij} is the center-to-center distance between an excitation patch j and receiving patch i. Note that quantity of radiated pressure instead of radiated force is adopted here, which is more convenient in calculating the radiated sound power as in Eq. (19).

APPENDIX D: DUCT RADIATION IMPEDANCE Z_d

Consider a semi-infinite rectangular duct excited by a vibrating surface at one end, the radiated sound pressure field using modal expansion method can be expressed as

$$p_d = \sum_s a_d^s \Psi_d^s, \tag{D1}$$

where a_d^s is the sth modal amplitude of the duct; the corresponding cross-sectional eigenfunctions corresponding to rigid side-walls are

$$\Psi_d^s = \cos\left(\frac{s_x\pi}{L_x^d}x\right)\cos\left(\frac{s_y\pi}{L_y^d}y\right), \quad s_x, s_y = 0, 1, 2, \ldots. \tag{D2}$$

In Ref. 19, the calculation of duct modal amplitude is given as

$$a_d^s = \rho_0 c_0 \sum_s \frac{1}{N_d^s \sin\theta} \int_{S_d} \bar{V}_n \Psi_d^s dS_d, \tag{D3}$$

where $\bar{V}_n$ is the normal vibrating velocity of the duct end, S_d is the surface area, $N_d^s = \int_{S_d} \Psi_d^s \Psi_d^{s'} dS_d$, and the modal phase angle

$$\sin\theta = -j\sqrt{\frac{[(s_x\pi/L_x^d)^2 + (s_y\pi/L_y^d)^2]}{(\omega/c_0)^2} - 1}. \tag{D4}$$

Then, according to Eq. (1), the duct radiation impedance is calculated as

$$Z_d = \frac{\bar{F}_i^d}{\bar{V}_j^d} = \rho_0 c_0 \sum_s \frac{1}{N_d^s \sin\theta} \int_{S_i} \Psi_d^s dS_i \int_{S_j} \Psi_d^s dS_j. \tag{D5}$$

[1] E. H. Dowell, G. F. Gorman, and D. A. Smith, "Acoustoelasticity: General theory, acoustic natural modes and forced response to sinusoidal excitation, including comparisons with experiments," J. Sound Vib. **52**, 519–542 (1977).
[2] C. R. Fuller and F. J. Fahy, "Characteristics of wave propagation and energy distribution in cylindrical elastic shells filled with fluid," J. Sound Vib. **81**, 501–518 (1982).
[3] J. Pan, C. H. Hansen, and D. A. Bies, "Active control of noise transmission through a panel into a cavity: I. Analytical study," J. Acoust. Soc. Am. **87**, 2098–2108 (1990).
[4] L. Cheng, Y. Y. Li, and J. X. Gao, "Energy transmission in a mechanically-linked double-wall structure coupled to an acoustic enclosure," J. Acoust. Soc. Am. **117**, 2742–2751 (2005).
[5] A. Dijckmans, G. Vermeir, and W. Lauriks, "Sound transmission through finite lightweight multilayered structures with thin air layers," J. Acoust. Soc. Am. **128**, 3513–3524 (2010).
[6] M. Ouisse, L. Maxit, C. Cacciolati, and J. L. Guyader, "Patch transfer functions as a tool to couple linear acoustic problems," J. Vib. Acoust. **127**, 458–466 (2005).
[7] J. D. Chazot and J. L. Guyader, "Prediction of transmission loss of double panels with a patch-mobility method," J. Acoust. Soc. Am. **121**, 267–278 (2007).
[8] M. Aucejo, L. Maxit, N. Totaro, and J. L. Guyader, "Convergence acceleration using the residual shape technique when solving structure-acoustic coupling with the Patch Transfer Functions method," Comput. Struct. **88**, 728–736 (2010).
[9] X. Yu, L. Cheng, and J. L. Guyader, "Vibroacoustic modeling of cascade panels system involving apertures and micro-perforated elements," in *20th International Congress on Sound and Vibration* (2013).
[10] L. Maxit, C. Yang, L. Cheng, and J. L. Guyader, "Modeling of micro-perforated panels in a complex vibro-acoustic environment using patch transfer function approach," J. Acoust. Soc. Am. **131**, 2118–2130 (2012).
[11] X. Yu, L. Cheng, and J. L. Guyader, "On the modeling of sound transmission through a mixed separation of flexible structure with aperture," J. Acoust. Soc. Am. **135**, 2785–2796 (2014).
[12] D. Y. Maa, "Potential of microperforated panel absorber," J. Acoust. Soc. Am. **104**, 2861–2866 (1998).
[13] J. Kang and M. W. Brocklesby, "Feasibility of applying micro-perforated absorbers in acoustic window systems," Appl. Acoust. **66**, 669–689 (2005).
[14] S. Allam and M. Åbom, "A new type of muffler based on microperforated tubes," J. Vib. Acoust. **133**, 031005 (2011).
[15] X. N. Wang, Y. S. Choy, and L. Cheng, "Hybrid noise control in a duct using a light micro-perforated plate," J. Acoust. Soc. Am. **132**, 3778–3787 (2012).
[16] T. Bravo, C. Maury, and C. Pinhède, "Sound absorption and transmission through flexible micro-perforated panels backed by an air layer and a thin plate," J. Acoust. Soc. Am. **131**, 3853–3863 (2012).
[17] T. Bravo, C. Maury, and C. Pinhède, "Vibroacoustic properties of thin micro-perforated panel absorbers," J. Acoust. Soc. Am. **132**, 789–798 (2012).
[18] J. Liu and D. W. Herrin, "Enhancing micro-perforated panel attenuation by partitioning the adjoining cavity," Appl. Acoust. **71**, 120–127 (2010).
[19] C. Wang, L. Cheng, J. Pan, and G. H. Yu, "Sound absorption of a micro-perforated panel backed by an irregular-shaped cavity," J. Acoust. Soc. Am. **127**, 238–246 (2010).
[20] C. Yang, L. Cheng, and J. Pan, "Absorption of oblique incidence sound by a finite micro-perforated panel absorber," J. Acoust. Soc. Am. **133**, 201–209 (2013).

[21]F. Sgard, H. Nelisse, and N. Atalla, "On the modeling of the diffuse field sound transmission loss of finite thickness apertures," J. Acoust. Soc. Am. **122**, 302–313 (2007).
[22]R. Panneton and N. Atalla, "Numerical prediction of sound transmission through finite multilayer systems with poroelastic materials," J. Acoust. Soc. Am. **100**, 346–354 (1996).
[23]A. Selamet and P. M. Radavich, "The effect of length on the acoustic attenuation performance of concentric expansion chambers: An analytical, computational and experimental investigation," J. Sound. Vib. **201**, 407–426 (1997).
[24]J. W. Lee and Y. Y. Kim, "Topology optimization of muffler internal partitions for improving acoustical attenuation performance," Int. J. Numer. Meth. Eng. **80**, 455–477 (2009).
[25]A. Selamet and Z. L. Li, "Acoustic attenuation performance of circular expansion chambers with extended inlet/outlet," J. Sound. Vib. **223**, 197–212 (1999).
[26]S. M. Kim and Y. H. Kim, "Structural-acoustic coupling in a partially opened plate-cavity system: Experimental observation by using nearfield acoustic holography," J. Acoust. Soc. Am. **109**, 65–74 (2001).
[27]H. Huang, X. Qiu, and J. Kang, "Active noise attenuation in ventilation windows," J. Acoust. Soc. Am. **130**, 176–188 (2011).
[28]C. Q. Howard, B. S. Cazzolato, and C. H. Hansen, "Exhaust stack silencer design using finite element analysis," Noise Control Eng. J. **48**, 113–120 (2000).
[29]W. L. Li, X. Zhang, J. Du, and Z. Liu, "An exact series solution for the transverse vibration of rectangular plates with general elastic boundary supports," J. Sound Vib. **321**, 254–269 (2009).
[30]J. T. Du, W. L. Li, H. A. Xu, and Z. Liu, "Vibro-acoustic analysis of a rectangular cavity bounded by a flexible panel with elastically restrained edges," J. Acoust. Soc. Am. **131**, 2799–2810 (2012).